# High-Resolution Radar Sensing Sea Surface States During AMK-82 Cruise

Alexey Ermoshkin and Alexander Molkov

***Abstract*—Every year situation when the Arctic seas are free of ice is becoming more frequent. It allows scientists to study hard-to-reach areas using well-equipped research vessels instead of icebreakers. During the COVID-19 pandemic, the successful expedition of the research vessel "Academician Mstislav Keldysh" with more than 60 scientists from 15 countries across the four Arctic seas (Barents, Kara, Laptev, and East Siberian) on September–November 2020 seems like a real wonder. One of the expedition tasks was remote sensing of different hydrophysical processes by their manifestation on the sea surface using marine radar. This article proposes the method of generating high spatial resolution radar maps of the sea surface and algorithms of hydrophysical processes identification. This article also presents examples of registered processes, such as wind waves, ice fields with different types of ice (grease ice, pancake ice, nilas, and young ice), manifestations of internal waves observed in the Kara Gate and Vilkitsky Strait, as well as manifestations of intense methane seeps on the sea surface. This article contains quantitative estimations of the physical parameters of the observed processes underlying the effectiveness of Doppler marine radars in harsh conditions of the Arctic seas.**

***Index Terms*—Arctic seas, doppler marine radar (DMR), ice, internal waves, methane seeps, radar detection, remote sensing, sea surface, wind waves.**

## I. Introduction

RADAR sensing of the sea surface is a convenient tool for obtaining information on the state of sea surface around the clock. Sea ice, swell and wind waves, atmospheric and oceanic fronts, internal waves, seep, and other surface manifestations of hydrophysical processes occurring at the ocean–atmosphere interface and in the water column can be registered using radar devices [1]–[4]. The most available data for radar sensing of the earth are Sentinel-1 radar data, which cover large areas [5]. However, the spatial resolution is not always sufficient to solve the inverse problem. For example, while the East Siberian Sea is covered by Sentinel-1 SAR images with a spatial resolution of 100 m, the generation and evolution of intense internal waves usually observed at the Vilkitsky Strait and the Kara Gate are interesting on scales of 20 m [6], [7]. Due to this, information on a large number of small-scale dynamic oceanological processes in the Arctic seas is not available.

Manuscript received December 25, 2021; revised March 14, 2022; accepted March 15, 2022. Date of publication March 22, 2022; date of current version April 8, 2022. This work was supported by the Russian Science Foundation under Project 20-77-10081. *(Corresponding author: Alexey Ermoshkin.)*

The authors are with the Institute of Applied Physics, Russian Academy of Sciences, 603950 Nizhny Novgorod, Russia (e-mail: eav@ipfran.ru; a.molkov@inbox.ru).

Digital Object Identifier 10.1109/JSTARS.2022.3161119

More regular and detailed information on these processes can be obtained using ship-based Doppler marine radar (DMR). The demonstrative results of using DMR from Helmholtz–Zentrum Geesthacht during a research cruise around the northern islands of the Republic of Palau on the research vessel (RV) Roger Revelle were presented in [1]. This article provides examples of manifestations of internal waves, zones of convergence currents, and surfactant films on DMR images. DMR, with its wide range, portability, and spatiotemporal capabilities, is an invaluable instrument for imaging of dynamic features of the upper ocean.

This article is based on the data of the *X*-band DMR Micran MRS-1000 of horizontal polarization [8], which was used in the 82nd scientific expedition of the RV "Academician Mstislav Keldysh" through four Arctic seas (Barents, Kara, Laptev, and East Siberian) on September–November 2020. The route of the expeditions began in Arkhangelsk and passed through the White and Barents Seas, the Kara Gate, the Kara Sea, the Vilkitsky Strait, the Laptev Sea, and the East Siberian Sea (see Fig. 1).

Long periods of open water are more and more often observed in this region. It leads to the occurrence of intense wind waves, changes in the processes of gas exchange between atmosphere and ocean, etc. According to studies [9], a lot of intense methane seeps are located on the shelves of the Laptev Sea and the East Siberian Sea. As a result, the contribution of the seeps to the region's climate is becoming more significant in the absence of ice cover.

However, there are positive aspects as well. For example, open water of the east Arctic enables scientists to study hard-to-reach areas using well-equipped RVs instead of icebreakers. Due to this opportunity, the data of each expedition seem especially important and valuable, which leads to expanding knowledge on the region under study.

On the path of more than 10 000 km, we registered wind waves of different intensities, ice fields with different types of ice (grease ice, pancake ice, nilas, and young ice), surface manifestations of internal waves, frontal zones, and methane seep manifestations on the sea surface.

A corresponding method for generating high spatial resolution radar maps of the sea surface and detecting mentioned hydrophysical processes on these maps is proposed in this article.

## II. Methods

### A. General Approaches

The reflection of microwave waves by a wavy sea surface is described by a two-scale (resonant) scattering model [10], [11],

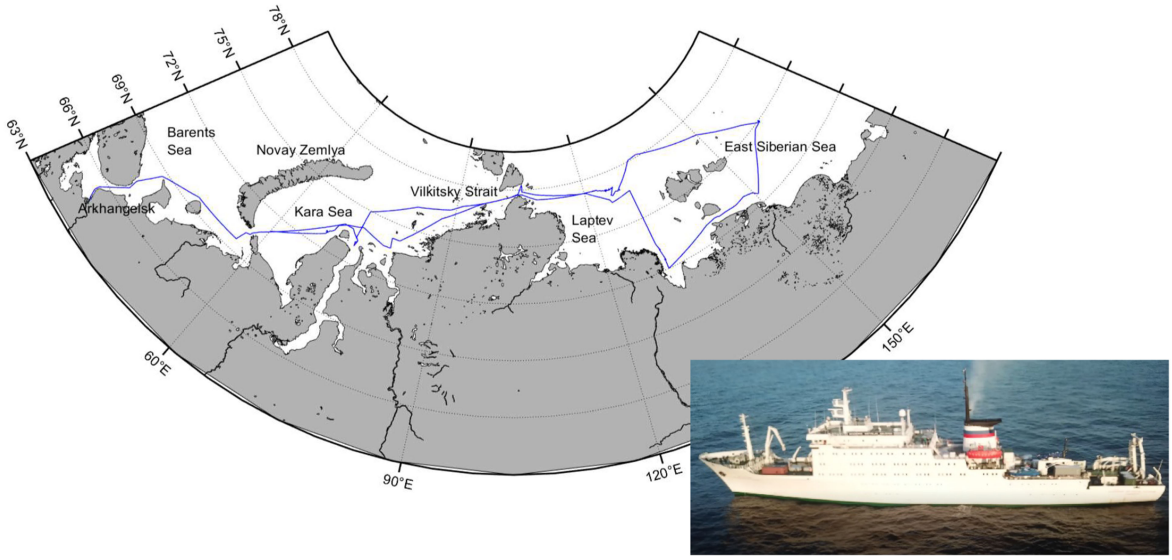


Fig. 1. RV "Academician Mstislav Keldysh" and its route on the 82nd cruise on September–November 2020.

which operates well at medium incidence angles common for the SAR satellite. For grazing angles typical of ship-based radars, an additional (nonresonant) scattering mechanism is required. It is usually related to the scattering on wave crests, breaking waves, and specular elements of the sea surface [12]. In this case, quantitative theoretical estimation of radar contrasts is extremely difficult due to the random nature of the processes that determine the level of scattered microwave waves. However, qualitative estimations are still possible.

Phenomena, such as internal waves, ocean fronts, vortex structures, and underwater gas jets, are manifested in radar signals due to variations in the sea surface roughness [13]. These variations are related to the transformation of wind waves on the current gradient, redistribution of surfactant films under the influence of flow, and the following effect of these films on short wind waves, as well as oceanic turbulence of different scales, which occurs, for example, in breaking of wind waves and internal waves, ship wakes, the current shift, and rising gas jets. In [1], the observation of subsurface processes on DMR images is related to the influence of inhomogeneous topography and is proposed to be used as a hazard indicator for navigation.

Detection and classification of ice types are also possible when analyzing radar images of the sea surface with SAR [14] or DMR [15]. In [15], the DMR of Helmholtz–Zentrum Geesthach, as well as in [1], is also used for ice detection in DMR images, however, ice-type classification was not posted. The results presented below illustrate the aforementioned phenomena in the Arctic seas, which are not visible in SAR images due to their small scale and inadequate resolution of the available SAR data.

### B. Radar Measurements

The X-band coherent DMR is an invaluable instrument for imaging of dynamic features of the upper ocean [1]. In contrast to Nyman *et al.* [1], we used a DMR MRS-1000 with horizontal radiation polarization. General technical parameters of DMR MRS-1000 are shown in Table I.

TABLE I
TECHNICAL CHARACTERISTICS OF DMR

| **Parameter** | **DMR MRS-1000** |
|---|---|
| Emitted radio power | 1 W |
| Frequency (wavelength) | 9.4 GHz (3.2 cm) |
| Maximum range with resolution 0.79 m | 3200 m |
| Beamwidth in horizontal plane | 1° |
| Beamwidth in vertical plane | 30° |
| Mode (modulation bandwidth) | Chirp modulation (*fm*=191.2 MHz) |
| Polarization (transmit / receipt) | Horizontal / Horizontal |
| Pulse length | 3.5 ms |
| Type of signal | Beat signal |
| Azimuth resolution | 0.5° |
| Range resolution | 0.79 m |
| Scanning mode | Circular and lateral |
| Rotation period | 2.5 s – 15 s |

This radar has a digital solid-state transmit/receive module following modern state-of-the-art broadband signal technology. Technical parameters of DMR MRS-1000 make it possible to detect and identify even small-sized objects, such as breaking waves, ice floats, buoys, etc., with high accuracy in all weather conditions 24/7.

On the 82nd scientific expedition, DMR was located on the highest deck at a height of 21.5 m. The observation range was 3200 m, range resolution, 0.79 m, and azimuth resolution, 0.5° (actual azimuth ground-projected resolution was from 1 to 10 m). Usually, DMR rotated a full 360°, but some measurements were conducted in lateral mode when it was mechanically fixed for a side looking. Radar data were obtained continuously with different frequencies (from 4 to 24 r/min) depending on the state of the sea surface.

When coherent radar operates from a board of moving vessels, it is necessary to consider the vessel velocity [16]. A corresponding method of determining the wave height from the side of a

moving vessel using Doppler measurements is proposed in [17]. For DMR MRS-1000, the range of unambiguously measured velocities is ±2.2 m/s, which is insufficient for measuring the velocities of the sea surface from a moving vessel. But in the case of the side look in the direction perpendicular to the motion direction, the additional velocity shift can be ignored. It makes it possible to determine wind wave spectra and surface current velocity [18], [19].

### C. Radar Data Processing

We obtained the brightness and Doppler radar images of the sea surface in polar coordinates for one rotation of the radar antenna: $I(\varphi, r, t)$, $V_d(\varphi, r, t) = \frac{\Delta\lambda}{4\pi\tau}$, where $\varphi$ is the azimuth angle, $r$ is the distance on the sea surface, $t$ is time, $\Delta$ is the pulse-to-pulse phase difference, $\lambda$ is the microwave wavelength, and $\tau$ is the pulse length. Two independent GPS dataset, including ship heading, velocity, and geographical coordinates ($cours(t)$, $u_{rv}(t)$, $\text{lat}_{rv}(t)$, $\text{lon}_{rv}(t)$) were used for considering RV orientation and motion. Incoherent signal averaging was employed to increase the signal-to-noise ratio. When the signal is averaged over space, the spatial resolution is lost. It can have a crucial effect on the detection of small objects or processes.

Due to the periodic scanning of space during the rotation of the radar antenna, noncoherent averaging over time becomes possible. For this purpose, the image $I(\varphi + cours(t), r, t)$ was converted to Cartesian coordinates $I(x, y, t)$, interpolated to a uniform grid with a step of 1 m, and converted to the normalized radar cross section

$$\sigma_0(x, y, t)[\text{dB}] = 10\log_{10}(A_c \cdot I(x, y, t)) \tag{1}$$

where $A_c$ is the calibration coefficient. Incoherent averaging was carried out over a time series of images on a common coordinate grid, where each image obtained in a single rotation covering an area ($x + \text{lat}_{rv}(t)$, $y + \text{lon}_{rv}(t)$) is determined by the following expression:

$$\langle \sigma_0(x, y) \rangle = \frac{1}{N} \sum_{i=1}^{N} \sigma_0 \left( x + \text{lat}_{rv}\left(t_i\right), y + \text{lon}_{rv}\left(t_i\right), t_i \right). \tag{2}$$

A similar processing method is implemented for satellite microwave scatterometers, according to which the velocity and direction of wind waves, precipitation, and the surface current velocity are determined. However, the microwave scatterometer cannot provide a detailed image, as SAR or DMR do. Analysis of detailed DMR images allows obtaining more complete information on oceanic processes occurring on the subgrid-scale of microwave scatterometers.

### D. Retrieval of the Parameters of the Hydrophysical Processes

By using coherent ship-based maritime radars, it is possible to quantify the physical characteristics of wind waves and current fields. Paper Nyman *et al.* [1] proposes methods of determining the velocity and direction of the current on the sea surface. An earlier paper [16] demonstrated this possibility. The wavefield can be described by statistical characteristics: significant wave height $H_s$, peak wavelength or period, and wave direction. By using incoherent marine radars and calibration dependences, $H_s$ is recovered, and the rest of the parameters are easily determined without additional calibration [20]. $H_s$ can also be easily determined on the basis of the DMR data [21], [22].

Inhomogeneous currents appear due to changes in the sea surface roughness and can manifest themselves in brightness and Doppler DMR images. Kinematic characteristics of processes, such as internal waves [6], convergence zones, and film slicks [23], are recovered due to the periodicity of the sea surface survey. The applications of radar sense to the problems of determining the spectrum of wind waves and the surface current velocity are described in [15], [18], [21], [22] and [1], [16], [19], [24], respectively.

Ice detection based on marine radar data is implemented by some manufacturers, for example, Rutter, Furuno, etc. An example of using MR and DMR for this purpose is given in [25] and [15], respectively. In addition to the ice detection, the issue of the ice classification is also important, especially for marine navigation and hydrometeorology. This issue is not solved in the cited papers. Therefore, this article proposes an approach that uses the joint information on brightness and Doppler radar images to extract features corresponding to packed ice, crushed ice, and open water.

And finally, we have not come across papers on employing marine radars for detecting manifestations of methane seeps on the wavy sea surface. Therefore, corresponding results of radar remote sensing of methane seeps on the sea surface are presented below for the first time.

There are some papers [26], [27] that provide the results of remote sensing of gas seeps in the Arctic. The authors consider the manifestations of seeps in optical sensing data, as well as in SAR images of the ice covering of Arctic lakes. One of the high-resolution DMR maps formed due to the application of the proposed method can be used to detect low-contrast subsurface processes, such as manifestations of methane seeps on the sea surface.

Thus, DMR helps to observe new features on the sea surface and recover the physical parameters of dynamic processes in the near-surface layer of the ocean during RV motion along the path without involving additional calibrations

## III. Results

### A. Wind Waves and Currents

We obtain a lot of information on the state of sea surface for significantly different meteorological conditions (wind velocity was up to 30 m/s). Examples of clearly visible wind waves on the brightness and Doppler radar panoramas in the distance-time coordinates obtained during the side view operation in the direction perpendicular to the vessel track are presented in Fig. 2(a) and (b). Their spectral characteristics obtained by applying 2-D FFT transformation to the given images are shown in Fig. 2(c). If only the kinematic characteristics of waves can be recovered from the brightness radar image, then the energy characteristics can also be determined from the Doppler radar image.

The sea surface current velocity can be determined using two approaches [1]. The first one uses the dispersion relation of waves on still water. The second approach employs the mean Doppler velocity, from which the wave and wind velocity

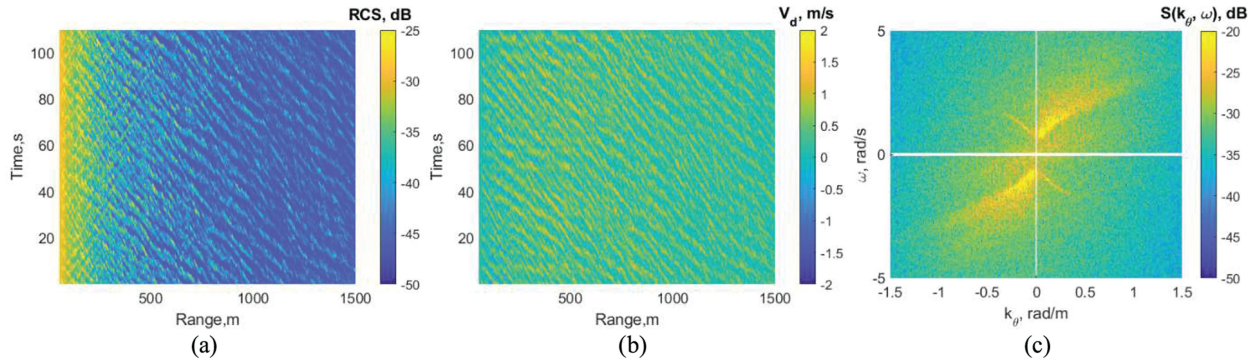


Fig. 2. (a) Radar brightness and (b) Doppler images of sea waves with a side view of DMR on the RV path and (c) Doppler images spectrum. Wind velocity - 8 m/s N, azimuthally looking direction – 40°.

components are subtracted. For this purpose, the DMR must have a wide range of unambiguously measurable Doppler velocities, minimum $\pm 10$ m/s. This is necessary to properly account for the velocity of the RV. In our case, the velocity of RV leads to a double aliasing of the Doppler velocity, which does not enable us to correctly analyze the results of measuring the Doppler velocity at angles different from the ones perpendicular to the ship's trajectory.

### B. Ice Fields

During the entire expedition, the ice fields were recorded only once, when the RV left the mouth of the Lena River. It was the beginning of ice forming. Fig. 3 shows a radar map consisting of different ice types [28]: open water, grease ice, pancake ice, and young ice. On the radar map obtained by the DMR, areas of young ice are clearly discernible, which give increased scattering and are characterized by sharp boundaries and structures. Areas of open water are characterized by anisotropic scattering with a smooth change in the level. Grease ice results in almost no backscattering. Pancake ice, as young ice, leads to an increased scattering level, but pancake ice also contains wave structures. In 2-D spectra of radar images of young ice [see Fig. 3(d)], wave components are completely absent, and wave components appear closer to the ice edge [see Fig. 3(c)], which indicates a decrease in ice concentration and a transition to pancake ice. The intensity and structure of the wave components in the 2-D spectra of radar images are different for open water [see Fig. 3(b)] and for an ice-covered surface [see Fig. 3(a), (c), and (d)], but they are considered here only to demonstrate the presence of wave structures that allow separation of the field-compacted and crushed ice.

The Doppler velocity of the scatterers, obviously, should also demonstrate singularities. To do this, at the bottom of Fig. 3, we present the mean $\langle V_d \rangle = \frac{\sum_N V_d}{N}$ and weighted mean $V_d^\sigma = \frac{\sum_i V_d^i \sigma^i}{\sigma}$ Doppler velocities on the region with an angular size of $5^\circ$ in the direction perpendicular to the left side of RV movement and from 100 to 200 m in range. Fig. 3 also contains the errors related to the influence of the ship's movement in this small region. It is clearly seen that the scatterer velocity increases significantly for open water area, whereas the scatterer velocity lies in the vicinity of zero areas in ice-covered areas. Although, strictly speaking, the ice fields drift, but under the conditions of observation from a moving vessel, which is also subject to drift due to the influence of wind and currents, such values are difficult to measure.

The closest available Sentinel-1A SAR image (see Fig. 4) shows a similar picture, but such images have the worst spatial resolution and are not always available. The black line corresponds to the RV path on the previous DMR map. As we can see, there is almost no open water on the RV path, the ice edge has shifted to the north. The time difference between DMR and SAR images is 48 h. However, the SAR image clearly shows grease ice, which looks like dark edges, but there is no way to see wave motion as a criterion of lack of ice cohesion. Thus, due to DMR, one can obtain ice maps on the ship's path. This makes it possible to refine the algorithms for classifying ice types.

### C. Internal Waves

The internal waves are often observed in straits and areas with complex topography [1]. The resolution of the available Sentinel satellite images is not sufficient to record such small-scale phenomena. On DMR maps, wave patterns are clearly discernible up to 3.2 km from the ship's path. Different-scale internal waves were recorded in the Kara Strait and the Velkitsky Strait.

Internal waves are studied in a large number of papers on radar, optical, and contact measurements. The main limitation of used data is their spatial and temporal resolution. For satellite information, especially in the Arctic regions, it is rarely possible to obtain time series of images of the same area of interest on the sea surface. Contact measurements are deprived of the possibility of high spatial resolution. The proposed method, in addition to the high spatial resolution, also has a high temporal resolution, namely, the gap between radar images used in the radar map formation is 15 s. As an example of the fine structure of internal waves registered during their generation in the Velkitsky Strait, the DMR map is shown in Fig. 5 (IW means an internal wave). Several systems of short-period internal waves with wavelengths less than 100 m and different propagation directions are observed. The Vilkitsky Strait is characterized by a complex bottom topography and strong currents, which apparently leads to the intense generation of short-period internal waves. The wave packet IW1 propagates in the southwest direction, which corresponds to the direction from the Kara Sea. In the IW1 train, up to seven waves are well distinguishable. Ahead of 2 km,

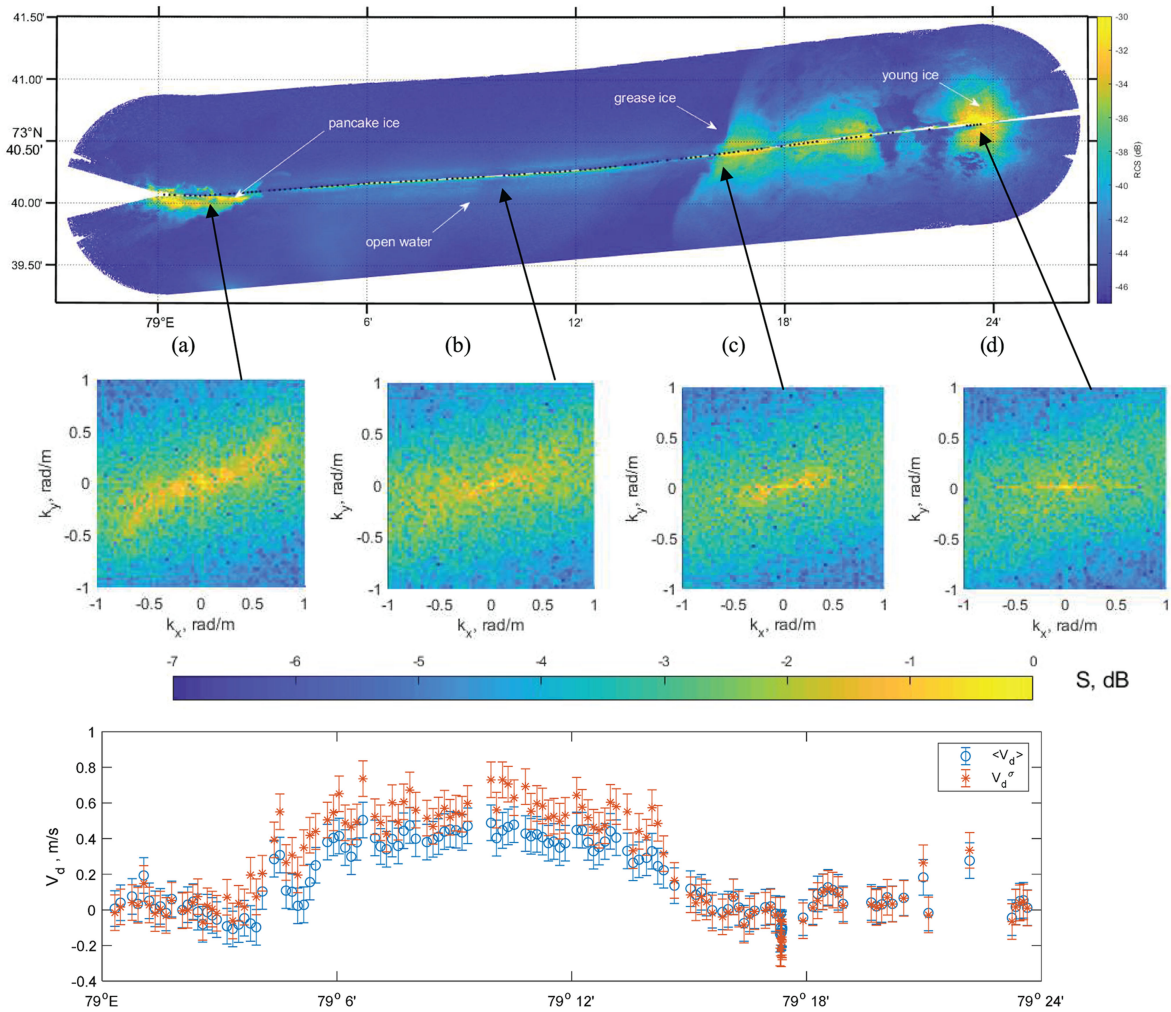


Fig. 3. DMR map of ice fields 26.10.2020 at 01:08 – 01:52 UTC (top), 2-D radar image spectra for different ice type (a, b, c, d), and Doppler velocity on the RV path for perpendicular to line-of-sight path (in the bottom image).

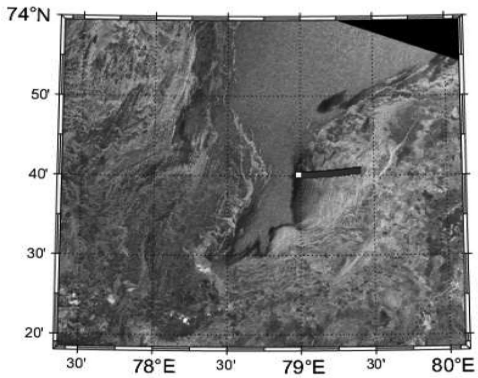


Fig. 4. Sentinel-1A SAR image 28.10.2020 at 01:54 UTC.

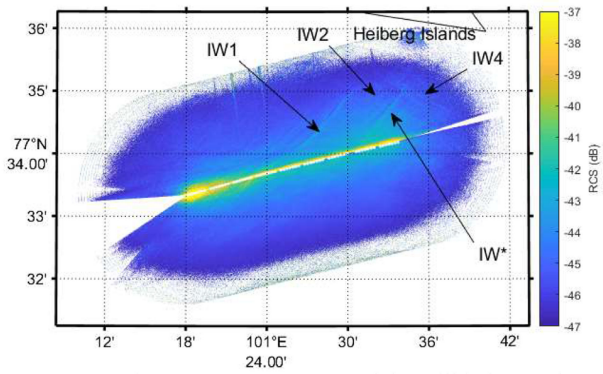


Fig. 5. Internal waves on DMR map of the Vilkitsky Strait.

the leading front IW∗ propagates in the same direction, which probably served as a source for the generation of weaker wave packets IW2 and IW3. Judging by the direction of propagation of IW2 and IW3, the possible place of generation may be the shelf of the Heiberg islands, which RV passed by at the time of receiving the DMR map in Fig. 5.

### D. Methane Seeps

Methane seeps are conventionally recorded during hydroacoustic measurements [9]. But in the case of a sufficiently intense release of methane bubbles, seeps can be observed by remote radar and optical systems through variations of the state of sea surface (see Fig. 6). Upon ascent, gas bubbles entrain the

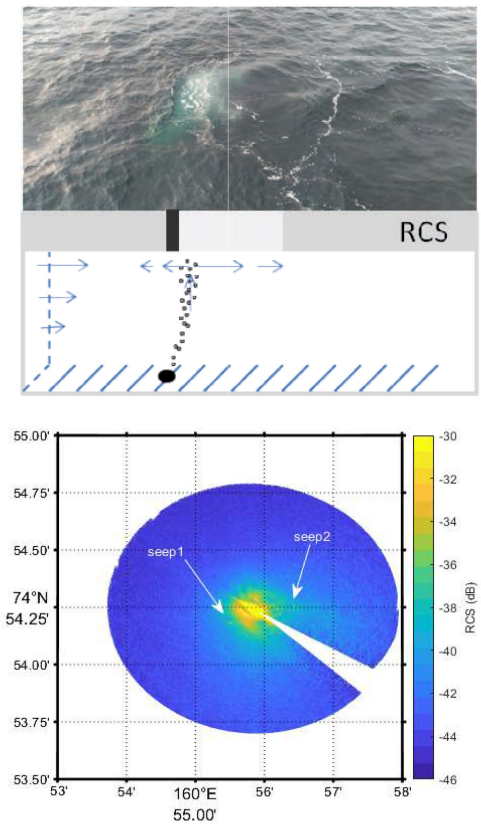


Fig. 6. Photo of surface manifestation methane seep at East-Siberian Sea and scheme of gas bubble jet (top), and example of seep manifestation on DMR image (bottom).

surrounding water forming an upward current. Reaching the sea surface, the current spreads in a thin surface layer isotropically, creating high flow velocity gradients. Therefore, oncoming wind waves are transformed: some of the waves dissipate due to the breaking, other waves are blocked and reflected, and the third part of waves bend around the region of inhomogeneous flow. As a result, on the windward side of the considered surface area, we observed increased surface roughness in comparison with the background sea surface due to the breaking intensification, steepening, and blocking of short wind waves by the oncoming flow. In the area of methane release to the surface, we observe an area of reduced roughness (slick). It relates to blocking, reflection, and refraction of the short-wave part of the wind wave spectrum in the region of the maximum gradient of the opposite current at the windward boundary of the seep and possible removal of surfactants. Also, small-scale turbulence with internal scales commensurate with the sizes of bubbles arises above the area of the rising gas jet. The emerging turbulent viscosity over the area where the gas jet exits to the surface leads to the damping of short-scale wind waves. Such a picture of the surface manifestation of methane seep on the sea surface can be registered remotely by marine radars. The dimensions of the methane seeps observed in the East-Siberian Sea were estimated visually by the size of the area occupied by gas bubbles near the surface, as no more than 2 m in diameter. Due to the formation of an inhomogeneous current area on the sea surface, the surface manifestation of the seep occupies a slightly larger size, about

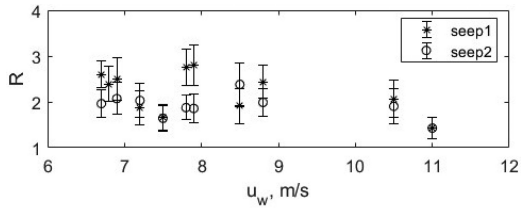


Fig. 7. Dependence of the radar contrast $R$ of manifestations of methane seeps on the sea surface on the wind velocity.

10 m, which can be determined from remote sensing data. The small scale of the phenomenon imposes significant requirements on the spatial resolution of remote equipment, which, apparently, was the reason for the complete absence of such data.

The value characterizing the level of reflected microwave energy is radar cross section $\sigma_0$. It depends on the sea surface roughness. As described earlier, there is a reduced roughness over the background roughness, resulting in values $\sigma_s^- < \sigma_0$. On the windward side of the seep area, there is an increased roughness related to the transformation of wind waves in the opposite current, therefore $\sigma_s^+ < \sigma_0$. When the radar is operating from a weakly drifting ship, the methane seep exit area is observed at the same or close azimuth angles. Fig. 6 shows a 10-min averaged radar panorama demonstrating qualitative reasoning, where we clearly see manifestations of two methane seeps.

The radar contrast of the hydrodynamic disturbance on the sea surface created by the methane release strongly depends on the observation geometry. As a numerical criterion for the observability of methane seep manifestations on the sea surface, we introduce the value $R$ equal to the ratio of the root-mean-square (rms) deviation of the value $\sigma_s$ in the area of the surface seep manifestation to the rms of $\sigma_0$ in a close but undisturbed surface area. The dependence of $R$ on wind velocity for two areas of methane seep manifestation on the surface is shown in Fig. 7. For one seep (seep1 in Fig. 6), located at a distance of about 150 m from the R/V, $R$ values were obtained higher than for the second seep (seep2 in Fig. 6), which was located at a distance of 350 m. In the case of weak and medium values of the wind velocity, the release of methane to the sea surface creates contrasts sufficient for radar detection, but with an increase in the wind velocity, hydrodynamic contrasts, as well as radar contrasts created by the release of methane to the sea surface, become weak and at a certain value of the wind are indistinguishable at all. This is due to an increase in the average value and variance of the quantity $\sigma_0$, as well as the flow velocity generated by the wind in the upper layer and the amplitude of the energy-carrying wave. It can be seen that as the wind velocity increases, $R$ decreases, which leads to the impossibility of remote radar sensing of the surface manifestation of the seep.

## IV. Conclusion

The presented results expand knowledge on hydrophysical processes in the Arctic seas and should be useful for the further development of remote monitoring systems especially marine radars. In addition to the well-known hydrophysical processes, we have shown its effectiveness for detecting small-scale

methane seeps on the Arctic shelf. They were detected by radar for the first time. The use of radar information from all ships in this region would make it possible to estimate the number of seeps, their intensity, and ultimately more accurately assess their integral contribution to the atmosphere and climate. The results obtained without loss of generality can also be applied to the development of methods of radar sensing of the Arctic seas by the SAR satellite.

Separately, it should be noted that obtained data and presented results are unique due to the inaccessibility of the region and its importance in connection with climate change [29].

## References


[1] L. Nyman, B. Lund, H. C. Graber, R. Romeiser, and J. Horstmann, "Radar observation of ocean surface features resulting from underwater topography changes," *Oceanography*, vol. 32, no. 4, pp. 174–183, Dec. 2019, doi: 10.5670/oceanog.2019.423.

[2] O. M. Phillips, "Radar returns from sea surface—Bragg scattering and breaking waves," *J. Phys. Oceanogr.*, vol. 18, pp. 1065–1074, 1988.

[3] F. Franco, "Enhanced ocean scatterometry," Ph.D. dissertation, Faculty Civil Eng. Geosci., Delft Univ. Technol, Delft, The Netherlands, 2015.

[4] A. A. Mouche, F. Collard, B. Chapron, K. F. Dagestad, G. Guitton, and J. A. Johannessen, "On the use of Doppler shift for sea surface wind retrieval from SAR," *IEEE Trans. Geosci. Remote Sens.*, vol. 50, no. 7, pp. 2901–2909, Jul. 2012.

[5] A. Moiseev, H. Johnsen, M. W. Hansen, and J. A. Johannessen, "Evaluation of radial ocean surface currents derived from Sentinel-1 IW Doppler shift using coastal radar and Lagrangian surface drifter observations," *J. Geophys. Res., Oceans*, vol. 125, 2020, Art. no. e2019JC015743.

[6] E. G. Morozov, V. T. Paka, and V. V. Bakhanov, "Strong internal tides in the Kara Gates Strait," *Geophys. Res. Lett.*, vol. 35, 2008, Art. no. L166603.

[7] I. E. Kozlov, E. V. Zubkova, and V. N. Kudryavtsev, "Internal solitary waves in the Laptev Sea: First results of spaceborne SAR observations," *IEEE Geosci. Remote Sens. Lett.*, vol. 14, no. 11, pp. 2047–2051, Nov. 2017.

[8] A. V. Ermoshkin, I. A. Kapustin, A. A. Molkov, N. A. Bogatov, and V. V. Bakhanov, "On the features of Doppler velocities estimation with coherent radar of high spatial resolution," in *Proc. SPIE 11150, Remote Sens. Ocean, Sea Ice, Coastal Waters, Large Water Regions*, Strasburg, France, 2019, Art. no. 111501I.

[9] J. Steinbach *et al.*, "Source apportionment of methane escaping the subsea permafrost system in the outer Eurasian Arctic Shelf," *Proc. Nat. Acad. Sci.*, vol. 118, no. 10, Mar. 2021, Art. no. e2019672118, doi: 10.1073/pnas.2019672118.

[10] G. R. Valenzuela and M. B. Laing, "Study of Doppler spectra of radar sea echo," *J. Geophys. Res.*, vol. 75, pp. 551–563, 1970.

[11] G. R. Valenzuela, "Theories for the interaction of electromagnetic and oceanic waves— A review," *Boundary Layer Meteorol.*, vol. 13, pp. 61–85, 1978, doi: 10.1007/BF00913863.

[12] V. Kudryavtsev, D. Hauser, G. Caudal, and B. Chapron, "A semiempirical model of the normalized radar cross-section of the sea surface, 1, background model," *J. Geophys. Res.*, vol. 108, no. C3, 2003, Art. no. 8054, doi: 10.1029/2001JC001003.

[13] V. Kudryavtsev, D. Akimov, J. Johannessen, and B. Chapron, "On radar imaging of current features: 1 Model and comparison with observations," *J. Geophys. Res.*, vol. 110, 2005, Art. no. C07016, doi: 10.1029/2004JC002505.

[14] N. Zakhvatkina, V. Smirnov, and I. Bychkova, "Satellite SAR data-based sea ice classification: An overview," *Geosciences*, vol. 9, no. 4, 2019, Art. no. 152, doi: 10.3390/geosciences9040152.

[15] J. Horstmann, J. Bödewadt, R. Carrasco, M. Cysewski, J. Seemann, and M. Stre$\beta$er, "A coherent on receive X-band marine radar for ocean observations," *Sensors*, vol. 21, 2012, Art. no. 7828, doi: 10.3390/s21237828.

[16] L. Nyman, B. Lund, R. Romeiser, H. Graber, and J. Horstmann, "A new approach to detect surface currents of complex flows using Doppler marine radar," in *Proc. Int. Geosci. Remote Sens. Symp.*, 2018, pp. 1493–1496, doi: 10.1109/IGARSS.2018.8519168.

[17] J. Cui, R. Bachmayer, B. de Young, and W. Huang, "Experimental investigation of ocean wave measurement using short-range K-band radar: Dock-based and boat-based wind wave measurements," *Remote Sens.*, vol. 11, no. 13, 2019, Art. no. 1607, doi: 10.3390/rs11131607.

[18] A. V. Ermoshkin and I. A. Kapustin, "Estimation of the wind-driven wave spectrum using a high spatial resolution coherent radar," *Russian J. Earth Sci.*, vol. 19, no. 3, 2019, Art. no. ES1005 1-9, doi: 10.2205/2019ES000662.

[19] A. V. Ermoshkin, I. A. Kapustin, A. A. Molkov, and N. A. Bogatov, "Determination of the sea surface current by a Doppler X-band radar (in Russian)," *Fundamentalnaya i Prikladnaya Gidrofizika*, vol. 13, no. 3, pp. 93–103, 2020, doi: 10.7868/S2073667320030089.

[20] W. J. Plant and G. Farquharson, "Origins of features in wave number-frequency spectra of space-time images of the ocean," *J. Geophys. Res.*, vol. 117, 2012, Art. no. C06015.

[21] R. Carrasco, M. Streßer, and J. Horstmann, "A simple method for retrieving significant wave height from Dopplerized X-band radar," *Ocean Sci.*, vol. 13, pp. 95–103, 2017, doi: 10.5194/os-13-95-2017.

[22] R. Carrasco, J. Horstmann, and J. Seemann, "Significant wave height measured by coherent X-band radar," *IEEE Trans. Geosci. Remote Sens.*, vol. 55, no. 9, pp. 5355–5365, Sep. 2017.

[23] I. A. Kapustin *et al.*, "On capabilities of tracking marine surface currents using artificial film slicks," *Remote Sens.*, vol. 11, no. 7, 2019, Art. no. 840, doi: 10.3390/rs11070840.

[24] N. Braun, F. Ziemer, A. Bezuglov, M. Cysewski, and G. Schymura, "Sea-surface current features observed by Doppler radar," *IEEE Trans. Geosci. Remote Sens.*, vol. 46, no. 4, pp. 1125–1133, Apr. 2008.

[25] M. V. Rohith, J. Jones, H. Eicken, and C. Kambhamettu, "Extracting quantitative information on coastal ice dynamics and ice hazard events from marine radar digital imagery," *IEEE Trans. Geosci. Remote Sens.*, vol. 51, no. 5, pp. 2556–2570, May 2013.

[26] V. G. Bondur and T. V. Kuznetsova, "Detecting gas seeps in arctic water areas using remote sensing data," *Izvestiya, Atmos. Ocean. Phys.*, vol. 51, no. 9, pp. 1060–1072, 2015, doi: 10.1134/S0001433815090066.

[27] V. I. Bogoyavlensky, I. V. Bogoyavlensky, T. N. Kargina, R. A. Nikonov, and O. S. Sizov, "Earth degassing in the Arctic: Remote and field studies of the thermokarst lakes gas eruption (in Russian)," *Arctic: Ecol. Economy*, vol. 2, no. 34, pp. 31–47, 2019, doi: 10.25283/2223-4594-2019-2-31-47.

[28] Introduction to Oceanography: 14.1 Types of ice, Bristol, RI, USA: Roger Williams Univ., 2021 [Online]. Available: https://rwu.pressbooks.pub/webboceanography/chapter/14-1-types-of-ice/

[29] S. Cardoso and J. Cartwright, "Increased methane emissions from deep osmotic and buoyant convection beneath submarine seeps as climate warms," *Nature Commun.*, vol. 7, 2016, Art. no. 13266.


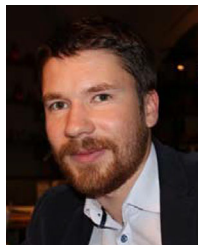

**Alexey Ermoshkin** received the B.S. degree and the M.Sc. degree in radiophysics from the Lobachevsky State University of Nizhny Novgorod, Nizhny Novgorod, Russia, in 2005 and 2007, respectively, and the Ph.D. degree in atmospheric and ocean physics from the Institute of Applied Physics of the Russian Academy of Sciences, Nizhny Novgorod, Russia, in 2017.

He is currently a Researcher with the Geophysical Research Division, Institute of Applied Physics, Russian Academy of Sciences, Nizhny Novgorod. His research interests include tasks of remote sensing, especially Doppler radar sensing of sea wind, waves, ice cover, currents, internal waves, and oil pollutions.

**Alexander Molkov** received the B.S. degree and the M.Sc. degree in radiophysics from the Lobachevsky State University of Nizhny Novgorod, Nizhny Novgorod, Russia, in 2007 and 2009, respectively, and the Ph.D. degree in atmospheric and ocean physics from the Institute of Applied Physics of the Russian Academy of Sciences, Nizhny Novgorod, Russia, in 2014.

He is currently a Senior Researcher with the Department of Radiophysical Methods in Hydrophysics, Institute of Applied Physics, Russian Academy of Sciences, Nizhny Novgorod, Russia. At the present moment, his experience counts 14 years in the remote sensing of physical processes in the upper water layer by their manifestations on the water surface. He has authored or coauthored more than 100 papers, including conferences proceedings.